ACS APPLIED MATERIALS & INTERFACES

Research Article

www.acsami.org

Gold-Coated Ordered Nanoporous Anodic Alumina Bilayers for Future Label-Free Interferometric Biosensors

Gerard Macias, Laura P. Hernández-Eguía, Josep Ferré-Borrull, Josep Pallares, and Lluís F. Marsal*

Departament d'Enginyeria Electrònica, Elèctrica i Automàtica, ETSE, Universitat Rovira i Virgili, Avda. Països Catalans 26, 43007 Tarragona, Spain

Supporting Information

ABSTRACT: A cost-effective label-free optical biosensor based on gold-coated self-ordered nanoporous anodic alumina bilayers is presented. The structure is formed by two uniform nanoporous layers of different porosity (i.e., a top layer with large pores and a bottom layer with smaller pores). Each layer presents uniform pore size, regular pore distribution, and regular diameter along its pore length. To increase and improve the output sensing signals, a thin gold layer on the top surface was deposited. The gold layer increases the refractive index contrast between the nanoporous alumina layer and the analytical aqueous solution, and it results in a greater contrast in the interferometric spectrum and a higher sensitivity of the structure. From this structurally engineered architecture, the resulting reflectivity spectrum shows a complex series of Fabry–Pérot interference fringes, which was analyzed by the reflective interferometric Fourier transform spectroscopy (RIFTS) method. To determine the performance of this structure for biosensing applications, we tested bovine serum albumin (BSA) as the target protein. The results show a significant enhancement of the RIFTS peak intensity and position when a gold layer is on the top surface.

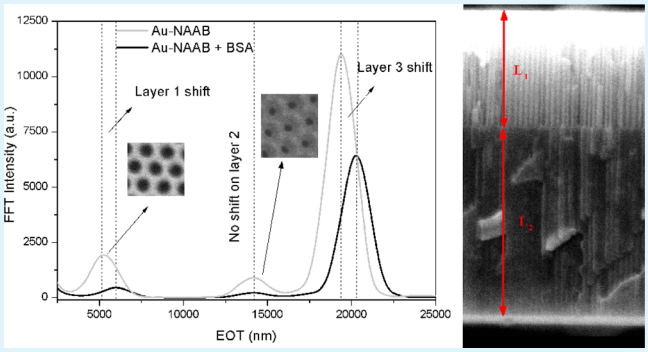

KEYWORDS: *nanoporous alumina, label-free biosensor, gold thin film, bilayer, Fabry–Pérot interference, fast Fourier transform*

1. INTRODUCTION

Over the past decade, biosensing has been subject of great interest in fields such as proteomics, biotechnology, medical diagnosis, pharmacy, and environmental sciences. To date, the most sensitive techniques are expensive, time consuming, and require fluorescent labels or molecular markers attached to the molecule of interest. The development of nanoporous materials, such as porous silicon (pSi) and nanoporous anodic alumina (NAA), offers the possibility to create cost-effective, highly sensitive, and fast-responding label-free optical biosensors. These materials present the advantages of a high surface area, size-selective molecular separation, and easy surface functionalization.[1−6] In a pioneering work, Sailor and Ghadiri reported the use of porous silicon as a label-free interferometric biosensor.[7] Recently, several label-free biosensors based on oxidized porous silicon single and double layers have been reported.[8−12] However, porous silicon shows limitations because of its instability in buffer solutions and degradation under both physiological and high pH conditions.[13−15]

A more interesting approach would be the use of nanoporous anodic alumina as a biosensor.[16−21] Alumina presents a higher stability at physiological pH,[22] and no passivation step is required. Moreover, by means of two-step anodization, it is possible to fabricate NAA with a self-ordered hexagonal pore arrangement.[23−25] The structural characteristics of NAA can be engineered to separate molecules of different sizes by adjusting the electrochemical etching conditions. The interpore distance is linearly proportional to the anodization potential, and the layer thickness is precisely controlled by the total charge passed through the electrodes.[26,27] Furthermore, pore diameters can be accurately enlarged by wet chemical etching in phosphoric acid.[28] Lately, pore modulation has been accomplished along the growth direction by different techniques, which allows for the development of more complex interferometric structures.[29−32]

Among optical methods, reflectometric interference Fourier transform spectroscopy (RIFTS) is one of the most sensitive.[10,18,20] This method is based on the interference of a white-light beam and a thin film. The pattern of the interferences depends on the effective optical thickness (EOT), which is defined as the product between the effective refractive index (n) and the thickness (L) of the thin film. Therefore, this technique is able to measure slight changes in the optical thickness of a thin film (i.e., the effective refractive index of a porous layer) using the variations in the interference patterns resulting from light reflection at the interfaces. However, when analyzing bilayers, this method encountered

Received: June 5, 2013
Accepted: July 22, 2013
Published: July 22, 2013

   dx.doi.org/10.1021/am4020814 | ACS Appl. Mater. Interfaces 2013, 5, 8093−8098

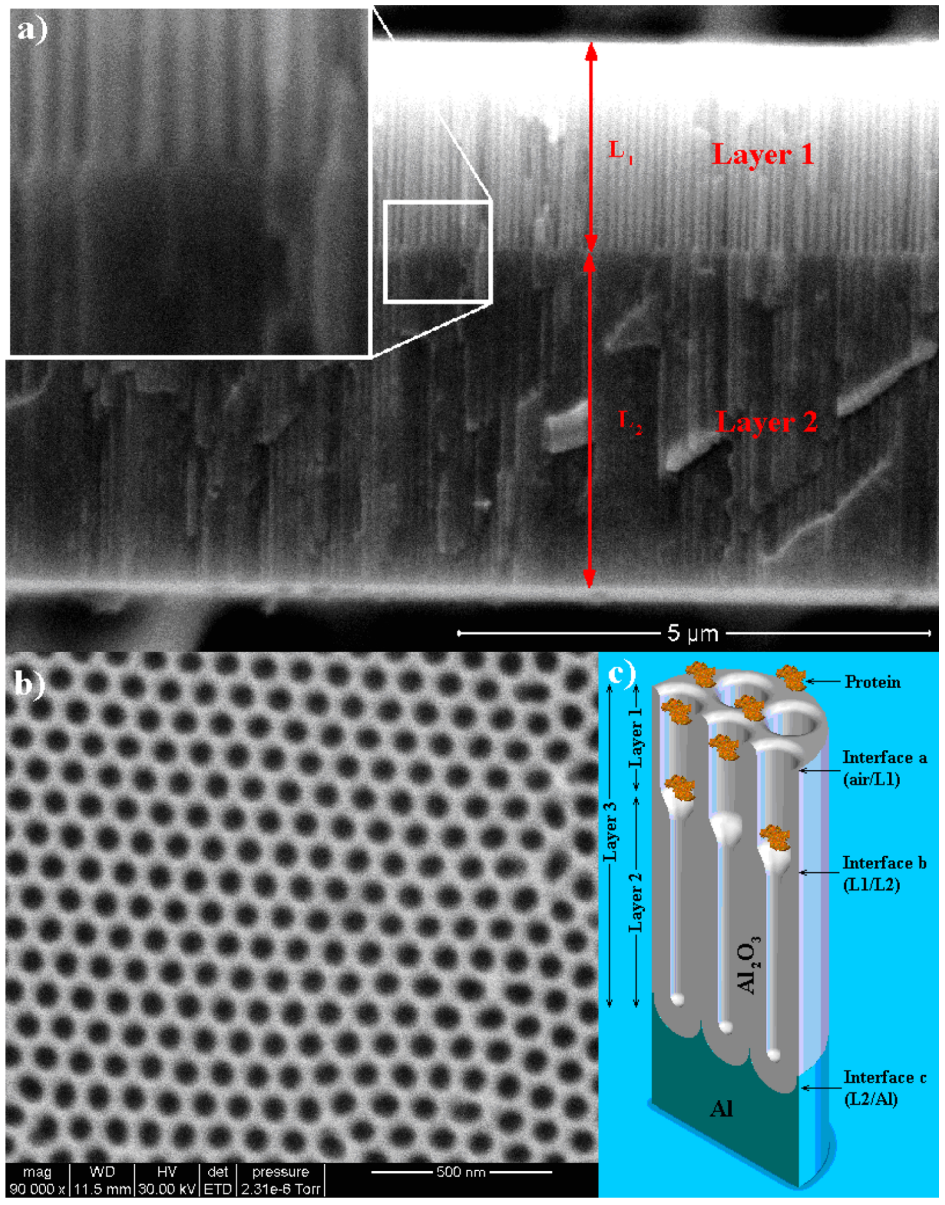

Figure 1. Scanning electron microscope (SEM) micrographs of (a) a cross-sectional view of the NAAB. The inset shows a magnification of the interface between the two layers displaying a funnel structure; (b) the top view of the NAAB. The top layer consists of a self-ordered hexagonal array of pores with a diameter of 68 nm and a thickness of 1.9 μm, whereas the bottom layer has a diameter of 33 nm and a thickness of 4.7 μm; (c) a schematic representation of the nanoporous anodic alumina bilayer. The interfaces a, b, and c represent the zone where the reflections occur resulting in three interfering light beams.

difficulties in the direct analysis of the top layer because of the low refractive index contrast at the first interface. One way to overcome this problem would be the deposition of a thin metal layer on top of the structure. A few nanometers of metal have been demonstrated to be an efficient approach for increasing the index contrast and consequently for enhancing the interference pattern.[18,19]

In this study, we present a gold-coated nanoporous anodic alumina bilayer (Au-NAAB) biosensor. This structure is formed by two uniform nanoporous layers of different porosities. The bottom layer (low porosity) is used as a blank for the in situ correction of the effect of bulk solution and other experimental fluctuations. The performance of this structure was tested with bovine serum albumin (BSA) as the target protein.

2. EXPERIMENTAL SECTION

NAA Fabrication. Nanoporous anodic alumina bilayers (NAAB) with large pore diameters on the top layer and small pore diameters on the bottom layer were prepared through an anodization procedure. The pore-size contrast is achieved by wet chemical etching after the second anodization step.

Self-ordered NAAB samples were produced by a two-step anodization procedure.[23,24] Commercial aluminum (Al) foils (99.999% and 500 μm thick) were purchased from Goodfellow Cambridge Ltd. Prior to anodization, an electropolishing treatment was performed in a mixture of ethanol (EtOH) and perchloric acid ($HClO_4$) (4:1, v/v) at 20 V for 4 min. Next, the first anodization step was carried out in an aqueous solution of 0.3 M oxalic acid ($H_2C_2O_4$) at 40 V and 4−6 °C for 20 h to achieve a self-ordering of the pores. The alumina layer with disordered pores was then selectively dissolved in a mixture of 6 wt % phosphoric (H_3PO_4) and 1.8 wt % chromic acid (H_2CrO_4) at 70 °C. Afterward, the second anodization step was

performed under the same conditions as the first step. The anodization time during this step was adjusted to obtain the desired pore length for the high-porosity alumina layer. Subsequently, the pore diameters were widened by wet chemical etching in an aqueous solution of 5 wt % H_3PO_4 for 15 min. Finally, a third anodization step was carried out under the same conditions as the first step to obtain a second low-porosity alumina layer (bottom layer).

Au-NAABs were obtained by depositing a 10 nm thick gold layer on top of the NAAB through sputtering under vacuum at 30 mA for 1 min using an EMITech K575X sputter coater.

BSA Infiltration. NAAB and Au-NAAB were initially incubated with 1 mg mL^{-1} of BSA in PBS for 2 h at 5 °C to avoid attachment of the proteins to the gold overlayer through thiol chemistry. Subsequently, the samples were thoroughly rinsed with PBS to remove any free BSA. Next, the samples were incubated again with a BSA solution (1 mg mL^{-1}) for 2 h at 5 °C for sensing. Prior to taking measurements, the remaining solvent was carefully removed to avoid the development of a protein layer on top of the structure, and the structure was left to dry in air for further reflectance measurements.

NAA Characterization. NAA samples were characterized by scanning electron microscopy (SEM FEI Quanta 600). A standard image-processing package (ImageJ, public domain program developed at the RSB of the NIH, USA) was used to perform the SEM image analysis. Reflectance spectra were obtained using a lambda 950 spectrophotometer from PerkinElmer (Whaltham, MA, USA) equipped with a tungsten lamp as the light source. The measurements were performed in the 350–600 nm range at quasi-normal incidence (6°).

3. RESULTS AND DISCUSSION

Figure 1a shows a representative SEM cross-sectional view of a nanoporous anodic alumina bilayer anodized in oxalic acid. The bilayer structure observed has large pore diameters on the top layer (layer 1) and smaller pore diameters on the bottom layer (layer 2). The cross section shows uniform straight nanopores for both layers, with layer thicknesses of ~1.9 and ~4.7 μm for layers 1 and 2, respectively. Figure 1b shows a top-view SEM image of the top NAA layer. As can be seen, the sample presents a well-ordered hexagonal distribution of pores with uniform size. A field-emission SEM cross section revealed no modification of the pore morphology after the sputtering of 10 nm of gold on top of the pores (Supporting Information). Figure 1c represents a schematic cross-sectional view of an NAAB biosensor where different thickness layers (L_1, L_2, and L_3) and three interfaces (a, b, and c) are indicated. The thickness of layer 3 is defined as $L_3 = L_1 + L_2$. The geometrical parameters, such as the pore diameters, interpore distances, and thickness were estimated from these SEM images. The Supporting Information summarizes the results.

In the design of these NAABs, it should be taken into account that the size of the nanopores of the top layer should allow for the entrance of the protein or substance to be sensed and the size of the nanopores of the bottom layer should be small enough to avoid the entrance of the aforementioned protein. If this condition is fulfilled, then the bottom layer of the NAAB can act as a blank for self-referencing the top layer.

Figure 2 shows reflectance spectra of two single nanoporous anodic alumina monolayers with different thicknesses ~1.9 and ~4.7 μm and of a nanoporous anodic alumina bilayer composed of both of the previous ones. The spectra show a series of oscillations that result from the diverse reflections of light at the various interfaces of the structure (i.e., Fabry–Pérot effect). For a single nanoporous alumina layer, the oscillation maxima can be described using the Fabry–Pérot equation

$$m\lambda = 2nL \tag{1}$$

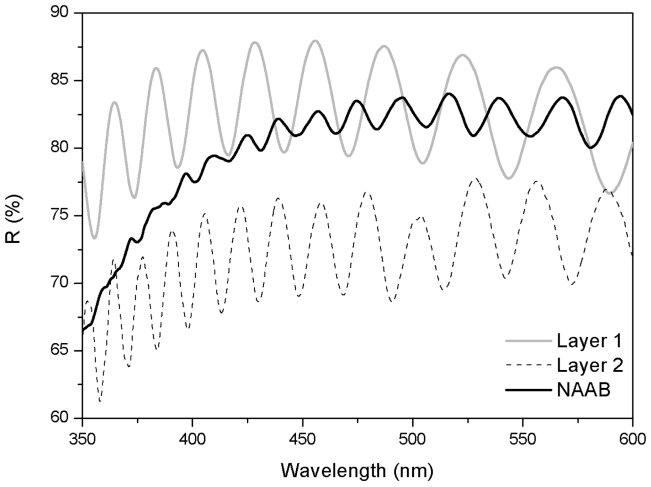

Figure 2. Reflectance spectra of two single nanoporous anodic alumina layers and a nanoporous anodic alumina bilayer. Layers 1 and 2 correspond to a 1.9 μm thick NAA sample of 41% porosity and a 4.7 μm thick NAA sample of 9% porosity, respectively. NAAB corresponds to a bilayer with layer 1 on top of layer 2.

where m is the order of the interference maximum, L is the thickness of the nanoporous anodic alumina layer, n is the effective refractive index, and λ is the wavelength of the incident light. The term $2nL$ refers to the effective optical thickness (EOT) of the NAA layer.

However, in the case of NAABs, the films display more complex oscillations than a mere single layer. This behavior can be fitted by a double-layer Fabry–Pérot model.[33]

$$R = (\rho_a^2 + \rho_b^2 + \rho_c^2) + 2\rho_a\rho_b \cos(2\delta_1) + 2\rho_b\rho_c \cos(2\delta_2) + 2\rho_a\rho_c \cos[2(\delta_1 + \delta_2)] \tag{2}$$

where δ_i represents the phase relationship of layer i

$$\delta_i = \frac{2\pi n_i L_i}{\lambda} = \frac{\pi}{\lambda}\mathrm{EOT}_i \tag{3}$$

and n_i represents the effective refractive index of layer i with thickness L_i. The factors ρ_a, ρ_b, and ρ_c are the Fresnel amplitude reflection coefficients, which are proportional to the refractive index contrast between the media surrounding corresponding interfaces a, b, and c (Figure 1c). Because n_1 and n_2 represent the effective refractive index of the top (layer 1) and bottom (layer 2) nanoporous alumina layers, respectively, and n_3 is defined as $(n_1L_1 + n_2L_2)/L_3$, any variation in the content of the nanopores will result in a change in their effective refractive index and therefore in the EOT and intensity of the interference oscillations. Furthermore, the amplitudes of the three cosine terms of eq 2 are also related to the index contrast at the two interfaces surrounding the layer

$$A_1 = k\rho_a\rho_b,\ A_2 = k\rho_b\rho_c,\ A_1 = k\rho_a\rho_c \tag{4}$$

where k is a proportionality constant that accounts for environmental variations such as lamp fluctuations or temperature drifts ($k = 2$ for the ideal case).

From these results and to extract the optical parameters of the NAAB, the fast Fourier transform (FFT) was used. Figure 3a shows the Fourier transform of the reflectance spectra of the NAAB in Figure 2. The EOT can be directly extracted from the FFT peak position. The results show that two peaks are observed at EOT_2 = 11 700 nm and EOT_3 = 16 700 nm, with

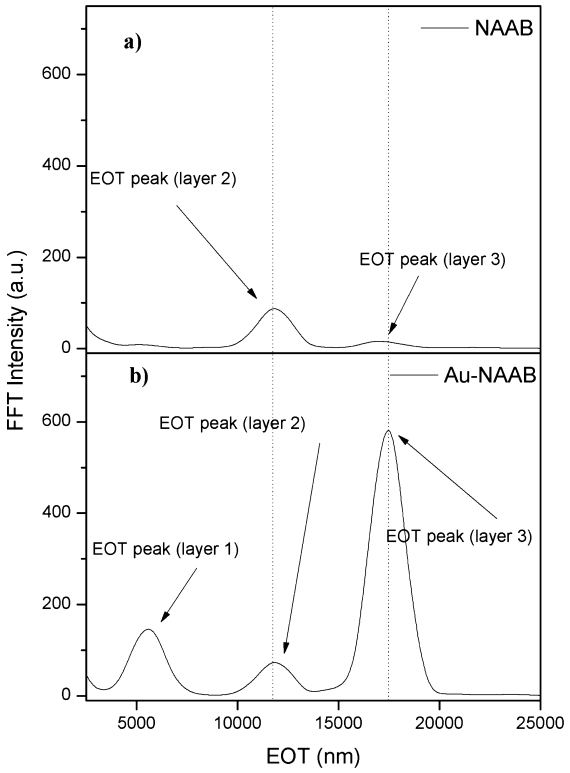

Figure 3. Comparison of the FFT plots of NAAB and Au-NAAB with the same layer 1 and layer 2 thicknesses. The deposition of the metal coating results in an enhancement of the FFT intensity of the layer 3 peak and the appearance of the layer 1 peak.

respective peak intensities of 85 and 15. These peaks correspond to the second and third cosine terms in eq 2. There should be also a peak at $EOT_1 \approx 5000$ nm, corresponding to layer 1, but its intensity is so small it can be hardly distinguished. This is a consequence of the small refractive index contrast at interfaces a and b.

Although the analysis of peaks 2 and 3 has been demonstrated to be enough for sensing, to improve the biosensor it would be desirable to obtain the information on peak 1. This can be accomplished by increasing the factors involved in A_1: ρ_a and ρ_b (i.e., by increasing the refractive index contrast at these interfaces). To do so, because interface b (between layers 1 and 2) is inaccessible, materials with a high refractive index can be deposited on top of NAABs to increase the index contrast at interface a. For such a purpose, metals like gold or silver are a great choice because of their optical properties.[34,35] However, the thickness of such metal layers should be designed carefully to avoid signal attenuation resulting from the absorption and occlusion of the nanopore. In the present work, gold (Au) was chosen not only for its optical properties but also for its biocompatibility.

Figure 3b shows the FFT intensity plot of the same NAAB as in Figure 3a after sputtering 10 nm of gold. The result shows a significant enhancement of the RIFTS peak intensity when the gold layer is on the top surface. As can be seen, three peaks are observed at $EOT_1 = 5856$ nm, $EOT_2 = 11\,700$ nm, and $EOT_3 = 17\,600$ nm, corresponding to layers 1, 2, and 3, respectively. Peak 1 is now visible because of the index contrast increase at interface a. Notice that the second peak intensity and position remains unaffected because interfaces b and c have not been modified. Finally, the third peak for layer 3 remains almost constant in position (~5% shift in EOT) but with a factor of 38 enhancement of its intensity because of the index contrast increase at interface a.

The incorporation of protein to the top layer can be detected by measuring the change in the optical thickness of layers 1 and 3 before and after the infiltration.

$$\Delta EOT = EOT(after) - EOT(before) \quad (5)$$

If the bilayered structure is correctly designed, no increment in the EOT of layer 2 should be noted after protein infiltration because of the size-exclusion phenomena. This effect allows us to use the EOT signal from layer 2 as a reference to correct the signal from both layers 1 and 3 as well as eliminates the effect of small molecules on the high-porosity layer.[12]

A complementary approach to detect the infiltration of protein in layer 1 is through the change of the FFT peak intensity. We can detect the infiltration of the protein by means of the peak amplitude ratios: $A_1/A_2 = \rho_a/\rho_c$ and $A_3/A_2 = \rho_a/\rho_b$. By using the amplitude of the FFT peak for layer 1, we can eliminate the k component of the amplitude equation that accounts for drifts resulting from lamp fluctuations or temperature drifts.

BSA is a common model protein used in biosensing. Its largest dimension is roughly 8 nm, and it is negatively charged at pH 7.[12] The diffusion of proteins into the pores can be significantly limited with pore diameters much larger than twice the hydrodynamic radius of the protein.[36] Therefore, no BSA should enter layer 2 even though its pore diameter is around 35 nm. During the experiment, the BSA adsorption to the NAA scaffold occurs because of electrostatic forces between the protein and the porous substrate.[16,12] In the case of the Au overlayer, the adhesion of BSA to gold could occur through the disulfide bonds present in the protein because gold is known for forming self-assembled monolayers with sulfur compounds.[18,20,35] For this reason, the structure was blocked with BSA before the sensing experiments.

Figure 4 shows the FFT plot of the Au-NAAB before and after the infiltration of BSA into the structure. In this figure, the reference Au-NAAB accounts for the bilayer after gold passivation with BSA. An overall decrease in the intensity of

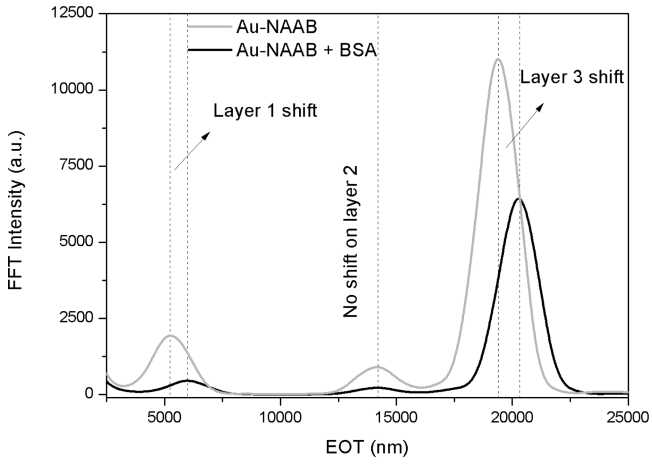

Figure 4. FFT plot of the optical response of the Au-NAAB before and after the introduction of the BSA protein. A decrease in the intensity of the FFT peak in all three layers is observed after the entrance of the BSA protein into the structure. The EOT only varies for layers 1 and 3 after the infiltration of the BSA protein.

Table 1. Experimental Results from the FFT Analysis of the NAAB and Au-NAAB before and after Being Infiltrated with BSA

sample	ΔEOT_1	ΔEOT_2	ΔEOT_3	A_1/A_2	A_3/A_2	A_1 (a.u.)	A_2 (a.u.)	A_3 (a.u.)
NAAB					1.27		2787	3554
NAAB + BSA		47	84		1.29		2766	3571
Au-NAAB				2.25	12.87	2310	1026	13 206
Au-NAAB + BSA	708	19	835	2.18	32.70	510	234	7652

the Fourier transform is observed. This is due to the adsorption of BSA in only layer 1, which increases its effective refractive index and consequently lowers the refractive index contrast of the overall structure. Furthermore, there is an increase in the EOT of both layers 1 and 3 because of the same reason, whereas the EOT of layer 2 remains almost unaltered. The small shift observed for layer 2 is a result of the resolution of the FFT algorithm as well as a small inhomogeneity of the sample (less than 1%). As can be seen, the variation of the EOT for layers 1 and 3 is 708 and 835 nm, respectively, after the infiltration. The same structure without gold deposition shows only the peaks for layers 2 and 3, and the variation of the EOT for the layer 3 is only 84 nm. These remarkable results indicate that the variation of the EOT for the Au-NAAB is an order of magnitude higher than the equivalent structure without the gold layer. It is also important to point out that there is no peak 1 (layer 1) for the NAAB structure without Au and the BSA is only sensed by means of peak 3, whereas for the Au-NAAB the BSA is sensed by means of peaks 1 and 3.

Regarding the ratio of the peak amplitudes, the analysis of the spectra of the Au-NAAB results in $A_1/A_2 = 2.25$ and $A_3/A_2 = 12.87$ before the infiltration of BSA, whereas $A_1/A_2 = 2.18$ and $A_3/A_2 = 32.70$ are obtained after the infiltration of BSA. In comparison with the structure without gold, these results represent an increase by a factor of 2.5 for peak 3. Table 1 summarizes the experimental results. These results prove that the gold deposition onto the NAAB increases considerably the response of the structure for biosensing.

4. CONCLUSIONS

This work has presented the fabrication and improvement in the sensing response of nanoporous anodic alumina bilayers in RIFTS applications by the deposition of a thin gold layer on top of the porous alumina layer.

This results in the appearance of the FFT peak corresponding to layer 1, which is hardly visible in bilayers without gold, and in the amplified intensity of the peak corresponding to the whole NAAB structure. This amplified response translates upon analyte adsorption into a more accurate determination of the change in the effective optical thickness and in a much bigger change in the FFT peak amplitude ratios.

Additionally, the existence of an additional clearly measurable peak permits a more self-consistent evaluation because of the redundancy of the data. Using BSA as a model protein, the deposition of the top thin Au layer results in an EOT shift 1 order of magnitude bigger than for the same NAAB structure without gold. Also, a change of the peak amplitude ratio by an increment of 2.5 times is achieved.

Further research needs to be done in relation to the biosensor sensitivity and to establish their full potential and practical utility. This system offers the possibility of developing a fast and low-cost miniature type of label-free biosensor for use as a reliable sensing system with applications in medicine, food analysis, and environmental monitoring.

■ ASSOCIATED CONTENT

Supporting Information

Structure characterization, SEM images, and detailed information on the experimental conditions used during the fabrication of NAAB and Au-NAAB samples. This material is available free of charge via the Internet at http://pubs.acs.org.

■ AUTHOR INFORMATION

Corresponding Author

*E-mail: lluis.marsal@urv.cat. Tel: +34 977559625. Fax: +34 977 559605.

Notes

The authors declare no competing financial interest.

■ ACKNOWLEDGMENTS

This work was supported by the Spanish Ministry of Economy and Competitiveness (MINECO) under grant no. TEC2012-34397 and the Government of Catalonia AGAUR 2009 SGR 549.

■ ABBREVIATIONS

OT = optical thickness
EOT = effective optical thickness
NAA = nanoporous anodic alumina
NAAB = nanoporous anodic alumina bilayer
Au-NAAB = gold-coated nanoporous anodic alumina bilayer
pSi = porous silicon
FFT = fast Fourier transform
BSA = bovine serum albumin
ESEM = environmental scanning electron microscope
RIFTS = reflectometric interference Fourier transform spectroscopy

■ REFERENCES

(1) Kilian, K. A.; Böcking, T.; Gooding, J. J. *Chem. Commun.* **2009**, *6*, 630−640.
(2) Jane, A.; Dronov, R.; Hodges, A.; Voelcker, N. H. *Trends Biotechnol.* **2009**, *27*, 230−239.
(3) Jani, A. M. M.; Losic, D.; Voelcker, N. H. *Prog. Mater. Sci.* **2013**, *58*, 636−704.
(4) Mäkilä, E.; Bimbo, L. M.; Kaasalainen, M.; Herranz, B.; Airaksinen, A. J.; Heinonen, M.; Kukk, E.; Hirvonen, J.; Santos, H. A.; Salonen, J. *Langmuir* **2012**, *28*, 14045−14054.
(5) Jani, A. M. M.; Kempson, I. M.; Losic, D.; Voelcker, N. H. *Angew. Chem., Int. Ed.* **2010**, *49*, 7933−7937.
(6) Velleman, L.; Triani, G.; Evans, P. J.; Shapter, J. G.; Losic, D. *Microporous Mesoporous Mater.* **2009**, *126*, 87−94.
(7) Lin, V. S.-Y.; Motesharei, K.; Dancil, K.-P. S.; Sailor, M. J.; Ghadiri, M. R. *Science* **1997**, *278*, 840−843.
(8) Pacholski, C.; Yu, C.; Miskelly, G. M.; Godin, D.; Sailor, M. J. *J. Am. Chem. Soc.* **2006**, *128*, 4250−4252.
(9) Furbert, P.; Lu, C.; Winograd, N.; DeLouise, L. *Langmuir* **2008**, *24*, 2908−2915.
(10) Orosco, M. M.; Pacholski, C.; Sailor, M. J. *Nat. Nanotechnol.* **2009**, *4*, 255−258.

(11) Pace, S.; Seantier, B.; Belamie, E.; Lautrédou, N.; Sailor, M. J.; Milhiet, P.-E.; Cunin, F. *Langmuir* **2012**, *28*, 6960−6969.
(12) Pacholski, C.; Sartor, M.; Sailor, M. J.; Cunin, F.; Miskelly, G. M. *J. Am. Chem. Soc.* **2005**, *127*, 11636−11645.
(13) Canham, L. T.; Reeves, C. L.; Newey, J. P.; Houlton, M. R.; Cox, T. I.; Buriak, J. M.; Stewart, M. P. *Adv. Mater.* **1999**, *11*, 1505−1507.
(14) Boukherroub, R.; Wayner, D. D. M.; Sproule, G. I.; Lockwood, D. J.; Canham, L. T. *Nano Lett.* **2001**, *1*, 713−717.
(15) Lees, I. N.; Lin, H. H.; Canaria, C. A.; Gurtner, C.; Sailor, M. J.; Miskelly, G. M. *Langmuir* **2003**, *19*, 9812−9817.
(16) Alvarez, S. D.; Li, C. P.; Chiang, C. E.; Schuller, I. K.; Sailor, M. J. *ACS Nano* **2009**, *3*, 3301−3307.
(17) Kumeria, T.; Parkinson, L.; Losic, D. *Nanoscale Res. Lett.* **2011**, *6*, 634−641.
(18) Kumeria, T.; Losic, D. *Nanoscale Res. Let.* **2012**, *7*, 88−98.
(19) Dronov, R.; Jane, A.; Shapter, J. G.; Hodges, A.; Voelcker, N. H. *Nanoscale* **2011**, *3*, 3109−3114.
(20) Santos, A.; Balderrama, V. S.; Alba, M.; Formentin, P.; Ferré-Borrull, J.; Pallarés, J.; Marsal, L. F. *Adv. Mater.* **2012**, *24*, 1050−1054.
(21) Santos, A.; Macias, G.; Ferré-Borrull, J.; Pallarés, J.; Marsal, L. F. *ACS Appl. Mater. Interfaces* **2012**, *4*, 3584−3588.
(22) Van Gestel, T.; Vandecasteele, C.; Buekenhoudt, A.; Dotremont, C.; Luyten, J.; Leysen, R.; Van der Bruggen, B.; Maes, G. *J. Membr. Sci.* **2002**, *207*, 73−89.
(23) Masuda, H.; Fukuda, K. *Science* **1995**, *268*, 1466−1468.
(24) Nielsch, K.; Choi, J.; Schwirn, K.; Wehrspohn, R. B.; Gösele, U. *Nano Lett.* **2002**, *2*, 677−680.
(25) Santos, A.; Montero-Moreno, J. M.; Bachman, J.; Nielsch, K.; Formentín, P.; Ferré-Borrull, J.; Pallarès, J.; Marsal, L. F. *ACS Appl. Mater. Interfaces* **2011**, *3*, 1925−1932.
(26) Lee, W.; Ji, R.; Gösele, U.; Nielsch, K. *Nat. Mater.* **2006**, *5*, 741−747.
(27) Santos, A.; Formentín, P.; Pallarès, J.; Ferré-Borrull, J.; Marsal, L. F. *J. Electroanal. Chem.* **2011**, *655*, 73−78.
(28) Zaraska, L.; Sulka, G. D.; Jaskula, M. *J. Solid State Electrochem.* **2011**, *15*, 2427−2436.
(29) Losic, D.; Lillo, M.; Losic, D. *Small* **2009**, *5*, 1392−1397.
(30) Lee, W.; Kim, J. C. *Nanotechnology* **2010**, *21*, 485304.
(31) Santos, A.; Vojkuvka, L.; Alba, M.; Balderrama, V. S.; Ferré-Borrull, J.; Pallarès, J.; Marsal, L. F. *Phys. Status Solidi A* **2012**, *209*, 2045−2048.
(32) Li, J.; Li, C. S.; Chen, C.; Hao, Q. L.; Wang, Z. J.; Zhu, J.; Gao, X. F. *ACS Appl. Mater. Interfaces* **2012**, *4*, 5678−5683.
(33) MacLeod, H. A. *Thin-Film Optical Filters*. Macmillan Publishing Co.: New York, 1986.
(34) Manickam, G.; Gandhiraman, R.; Vijayaraghavan, R. K.; Kerr, L.; Doyle, C.; Williams, D. E.; Daniels, S. *Analyst* **2012**, *137*, 5265−5271.
(35) Spadavecchia, J.; Casale, S.; Boujday, S.; Pradier, C.-M. *Colloids Surf., B* **2012**, *100*, 1−8.
(36) Gutenwik, J.; Nilsson, B.; Axelsson, A. *J. Chromatogr., A* **2004**, *1048*, 161−172.